metals

MDPI

Article

Hybrid Zinc Coatings with Improved Corrosion Resistance Based on Chitosan Oligosaccharides

Nelly Boshkova [1], Georgy Grancharov [2], Maria Shipochka [3], Georgy Avdeev [1], Stela Atanasova-Vladimirova [1], Olya Stoilova [2] and Nikolai Boshkov [1,*]

[1] Institute of Physical Chemistry "R. Kaishev", Bulgarian Academy of Sciences, "Acad. G. Bonchev" St. Bl. 11, 1113 Sofia, Bulgaria; nelly.boshkova@ipc.bas.bg (N.B.); g_avdeev@ipc.bas.bg (G.A.); statanasova@ipc.bas.bg (S.A.-V.)
[2] Institute of Polymers, Bulgarian Academy of Sciences, "Akad. G. Bonchev" St. Bl. 103A, 1113 Sofia, Bulgaria; granchar@polymer.bas.bg (G.G.); stoilova@polymer.bas.bg (O.S.)
[3] Institute of General and Inorganic Chemistry, Bulgarian Academy of Sciences, "Acad. G. Bonchev" St. Bl. 11, 1113 Sofia, Bulgaria; shipochka@svr.igic.bas.bg
* Correspondence: nboshkov@ipc.bas.bg

Abstract: In this paper, hybrid coatings based on ZnO dispersion in water soluble chitosan oligosaccharides (COS) as dispersion medium were prepared. The obtaining procedure of anti-corrosion hybrid zinc-based coatings containing COS coated ZnO particles in the metal matrix has been described. The available ZnO particles coated with COS were observed by TEM and thereafter added to the starting electrolyte for electrodeposition of hybrid zinc coatings on low-carbon steel substrates. The newly developed objects were collated with ordinary zinc coatings concerning the peculiarities of the morphology, topography and hydrophilicity of the surface (SEM and AFM analyses, water contact angle measurements), as well as corrosion behavior and electrochemical characteristics (cyclic voltammetry, potentiodynamic polarization curves, polarization resistance measurements). XRD and XPS methods were applied for studying of the crystallographic structure, as well as chemical and phase composition of the newly appeared corrosion products during the corrosion treatment in the test medium. Protective parameters of the coatings were evaluated in chloride environment of 5% NaCl solution. The results showed the effect of the concentration of the COS coated ZnO particles on the crystallographic structure and on the anticorrosion stability of the hybrid coatings.

Keywords: hybrid zinc coatings; corrosion; chitosan oligosaccharides; ZnO

Citation: Boshkova, N.; Grancharov, G.; Shipochka, M.; Avdeev, G.; Atanasova-Vladimirova, S.; Stoilova, O.; Boshkov, N. Hybrid Zinc Coatings with Improved Corrosion Resistance Based on Chitosan Oligosaccharides. *Metals* **2024**, *14*, 636. https://doi.org/10.3390/met14060636

Academic Editor: Petros E. Tsakiridis

Received: 7 May 2024
Revised: 23 May 2024
Accepted: 24 May 2024
Published: 27 May 2024

1. Introduction

The corrosion degradation of metals and alloys is undesirable process which may cause serious safety and environmental problems accompanied with economic loses. This is very dangerous for the steels, especially for the low-alloyed ones. Traditionally, the latter are widely applied in many branches—transport industry, building industry, bridge and railway constructions etc. Due to the presence of various chemical and other pollutants in the water, soil and air as well as due to climate changes the application of mild steels often leads to significant financial expenses. The reason for this is the urgent need of cheap and increased protection measures against corrosion destruction [1,2].

This dangerous process is often a result of the interaction of the metals with chloride ions from the surrounding environment [3]. One possible way to reduce the corrosion damages is the usage of low-carbon steels with accessorial protection based on corrosion resistive coatings (metallic, alloy, hybrid etc.) or conversion films. The application of protective coatings has an important role for the decreasing of the damages since it leads to a safety barrier against the aggressive surrounding media. Generally, these coatings distinguish with relatively low cost and good mechanical strength. One economically favorable possibility for safe corrosion protection of mild steel is the galvanizing [4,5].

Zinc coatings are widely used for corrosion protection since this metal is more active than iron, i.e., it demonstrates a sacrificial action during the corrosion process [6]. Nowadays it is well-known practice to substitute the zinc coatings with composite or hybrid ones [7,8]. The embedding of different metal, oxide, polymer or other particles meliorates the protective characteristics of the usual zinc coatings [9–17]. The particles incorporated in the metal matrix can fill some of the micro-holes, pores, gaps, or other surface coatings defects which could act as active sites for corrosion development. They also are to a certain degree a physical barrier minimizing in such a way the appearance of corrosion process. This statement is based on the additional formation of "mixed" barrier layers the latter containing corrosion products with low solubility and the incorporated particles [18].

A promising solution to enhance the corrosion resistance of zinc is to coat its surface with protective film of natural polymers [19,20]. Among natural polymers, chitosan is very promising not only because of its biocompatibility and biodegradability, but also because of its good film-forming and binding ability, as well its adhesion [21,22]. Chitosan is a deacetylated derivative of chitin—the second most abundant renewable biopolymer after cellulose. However, chitosan is not a homopolymer and apart from β(1→4)-linked D-glucosamine units it also contains β(1→4)-linked N-acetylglucosamine units. As a polycationic polysaccharide, due to the presence of reactive amino groups, chitosan is soluble only at acidic pH. In particular, the presence in the structure of chitosan of reactive functional groups (hydroxyl and amino groups) capable of chelating various metal ions (Cu, Fe, Ni, Zn, Pb, Mn), predetermines its ability to form complexes with them. In addition, chitosan might be deposited on metal electrodes by electrodeposition, forming a thin protective film. Recently, chitosan oligosaccharides (COS) prepared by chemical or enzymatic hydrolysis of chitosan, provokes special interest. In addition to the beneficial physical and biological properties of chitosan, COS also has a number of advantages over it, but the main is its excellent water solubility, regardless of the pH of the medium. Therefore, the usage of COS as dispersing agent of ZnO is an elegant solution to create a protective anti-corrosion coating by electrochemical deposition.

The present manuscript focuses on the obtaining of combined anticorrosion effect of COS and ZnO. The obtained hybrid coatings with incorporated COS and ZnO particles were electrodeposited on low carbon steel substrates to protect them from chloride caused corrosion attack. The effect of the COS coated particles as active anticorrosion components has been evaluated in comparison to the ordinary zinc coating.

2. Materials and Methods

2.1. Materials

Commercially available chitosan oligosaccharides (COS, 10,000 g/mol, Kitto Life Co., Ltd., Seoul, Republic of Korea) and zinc oxide nanopowder (ZnO, Zano®20, Umicore Zinc Chemicals, Brussels, Belgium) were used as received. The rodlike ZnO particles size was about 10–30 nm in diameter and 100 nm in length with bulk density of 280 g/L and specific surface area (BET) of 25–35 m^2/g.

2.2. Preparation of Dispersions to Obtain Hybrid Coatings

In order to obtain suitable dispersions, ZnO nanopowder (20 wt.% and 40 wt.% with respect to COS) was added to the aqueous COS solution (0.1 wt.%). The obtained dispersions were homogenized by sonication for 1 h in an ultrasonic bath (Bandelin Sonorex, Berlin, Germany, 160/640 W, 35 kHz).

2.3. TEM Studies

The obtained ZnO/COS dispersions were observed by high-resolution Scanning Transmission Electron Microscopy HR STEM JEOL JEM 2100 (JEOL Ltd., Tokyo, Japan) operating at a voltage of 200 kV and equipped with the Selected Area Electron Diffraction (SAED). Samples were prepared by drop-casting of the ZnO/COS dispersion onto a copper grid covered with formvar, followed by solvent evaporation.

2.4. Electrodeposition of the Hybrid Coatings

Zinc and two types of hybrid zinc-based coatings were electrodeposited on low-carbon steel plates with sizes 2 cm × 1 cm × 0.1 cm. The starting electrolytes have the following composition: 150 g/L of $ZnSO_4 \cdot 7H_2O$, 30 g/L of NH_4Cl, 30 g/L of H_3BO_3, as well as wetting agent AZ1 (50 mL/L), brightener AZ2 (2 mL/L) and pH value in the range 4.5–5.0. Two different concentrations (described below) of COS-coated ZnO particles as dispersion were added to the electrolytes. The electrodeposition has been carried in out glass cell (volume 600 ml) at ambient temperature, cathode current (direct current) density of 2 A/dm^2 and metallurgical zinc anodes. All the coatings obtained had equal thickness of ~12 μm. After the end of the electrodeposition the samples were subtracted from the experimental bath and dried in air. The obtained hybrid coating types are designated as follows:

- COS1—hybrid coatings electrodeposited from a starting electrolyte with a concentration 0.02 wt.% ZnO;
- COS2—hybrid coatings electrodeposited from a starting electrolyte with a concen tration of 0.04 wt.% ZnO.

2.5. Surface Morphology

The characteristics of the surface morphology and the distribution of the incorporated COS-coated ZnO particles in both hybrid coatings were observed with Scanning Electron Microscopy device (INCA Energy 350 unit, Oxford, UK).

2.6. Corrosion Characterization and CVA Studies

In order to obtain valuable and realistic information concerning the protective ability and electrochemical parameters of the investigated hybrid coatings, two well-known experimental methods were used—potentiodynamic (PDP) polarization curves (as accelerated method) and polarization resistance (Rp) measurements during a prolonged time interval. The corrosion data received from these methods was compared with the data of ordinary zinc coating. The electrochemical processes occurring in the cathodic and anodic regions were investigated with Cyclic Voltammetry (CVA) in the starting electrolytes. A PAR "VersaStat 4" device was applied for the experiments. Saturated Calomel Electrode (SCE) was chosen as the reference electrode, and a platinum plate was the counter one. During the PDP tests, a visual observation by the "naked eye" indicates the state of the sample, and after the appearance of bare steel substrate, the anodic polarization was stopped. The Rp measurements have been carried out for a period of 45 days. The studies with Cyclic Voltammetry (CVA) were pursued between −1.4 V and 0 V potential interval with a scan rate of 10 mV/s.

2.7. Atomic Force Microscopy (AFM) and Water Contact Angle Measurements

A Bruker Dimension Icon AFM microscope (Santa Barbara, CA, USA) working under ST mode was applied for the obtaining of samples surface topography. The images were analyzed in air at room temperature applying silicon tips (RTESPA) with resonance frequency of approx. 300 kHz, spring constant 40 N/m, and a scan rate of 1.0 Hz. The water contact angle (WCA) of the obtained coatings was determined at room temperature using a DSA20E Drop Shape Analyzer (KRÜSS GmbH, Hamburg, Germany). The contact angle was measured using the image of a sessile droplet of distilled water (10 μL), deposited by a computer dosing system onto the hybrid coatings surface, at the points of intersection between the drop contour and the projection of this surface (baseline). By DSA1 software (v 1.92-05), the average WCA was calculated by measuring at least 5 droplet images for each sample.

2.8. Chemical and Phase Composition (XPS Analysis)

The XPS measurements were performed in VG ESCALAB II (Seattle, WA, USA) electron spectrometer using AlKα radiation with an energy of 1486.6 eV. C1s line at 285 eV

(from an adventitious carbon) with an accuracy of ±0.1 eV as a reference was used to determine the binding energies. The chemical composition of the films was evaluated having in mind the areas and binding energies of C1s, O1s, Zn2p, Cl2p and Na1s photoelectron peaks (after linear subtraction of the background) and Scofield's photoionization cross-sections.

2.9. XRD Analyses

X-ray diffraction analysis was applied to define the phase composition and metallographic orientation of the electrodeposited hybrid coatings by using of X-ray diffractometer (CuKα radiation; generator voltage 40 kV), equipped with a PW1830 generator and a PW1050 goniometer manufactured by Philips (Amsterdam, The Netherlands). Data were obtained in the angular range of 10–60° 2-theta with a step of 0.05° 2-theta and exposure of 3 s. HighScore Plus 3.0 program, Inorganic Crystal Structure Database (ICSD) and Powder Diffraction File™ (PDF-2 2023) were performed for the phase analysis.

2.10. Corrosive Medium and Reproducibility of the Investigation Results

Electrochemical and corrosion experiments were realized in a model medium of 5% NaCl solution (pH ~6.7). The results were summarized as an average from the data obtained of five samples per type, i.e., either ordinary zinc or hybrid zinc coatings with COS-coated ZnO particles.

3. Results

3.1. TEM Studies

In the present study, stable ZnO/COS dispersions were used to create a protective anti-corrosion coating on low-carbon steel by electrochemical deposition method. In particular, hydroxyl and amino groups of COS form a coordination bond with Zn-ions, thus stabilizing ZnO/COS dispersion [23]. Moreover, the polycationic COS adsorbed on the ZnO surface due to electrostatic attraction between the negative surface of ZnO particles and positively charged COS. Finally, the film-forming ability of COS also had an influence on the properties of the protective anti-corrosion coating (Figure 1).

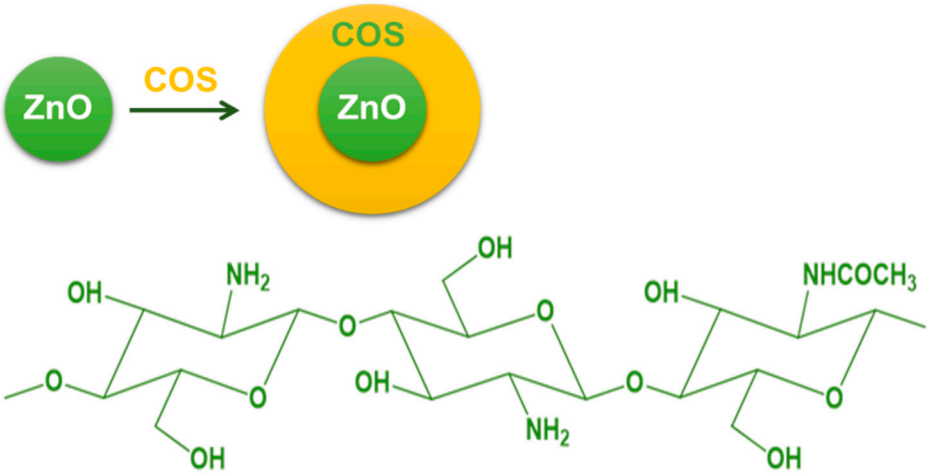

Figure 1. Schematic representation of COS-coated ZnO particles and chemical structure of COS.

The successful coating of the rodlike ZnO particles with COS was observed by HR-TEM equipped with SAED (Figure 2). Obviously, the addition of rodlike ZnO particles into aqueous COS solution results in the formation of shell onto the particles surface (Figure 2a). The SAED patterns (Figure 2b) showed the strong and bright diffraction spots that evidence the lattice spacing of the crystals, indexed to the hexagonal structure of ZnO with a = 3.24900 Å and c = 5.20700 Å [COD Entry #96-901-1663].

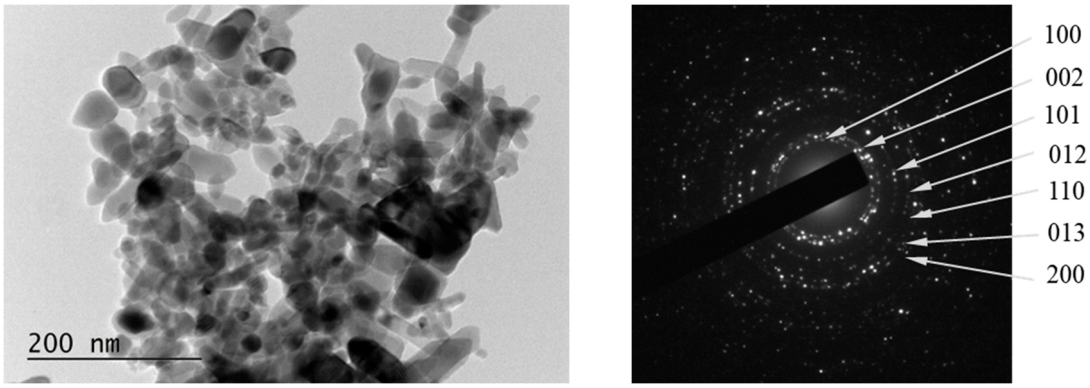

(**a**) (**b**)

Figure 2. TEM images (**a**) and SAED patterns (**b**) of ZnO/COS.

3.2. Surface Morphology

Scanning Electron micrographs micrographs of COS1 and COS2 hybrid coatings (as received) are presented in Figure 3a,c. Obviously, both samples are distinguished by relatively uneven and partially rough surfaces. However, the surface morphology of the COS1 sample seems to be more even and smooth compared to the COS2 one, which is characterized with greater inhomogeneity. Some individual white spheres appear on the surfaces of both sample types, indicating the presence of the incorporated COS-coated ZnO particles. The changes in the surfaces of the hybrid coatings after their prolonged stay in the experimental test medium of 5% NaCl solution are shown in Figure 3b,d. Both samples are covered with a layer of corrosion products, the latter being more even and smooth in the case of COS1. As is well known from our other investigations, the main corrosion product after such kind of treatment is zinc hydroxide chloride ZHC [14,18,24]. This compound has low solubility and takes part in the corrosion protection by forming a "mixed" layer containing simultaneously ZHC from the dissolution process and COS-coated ZnO particles.

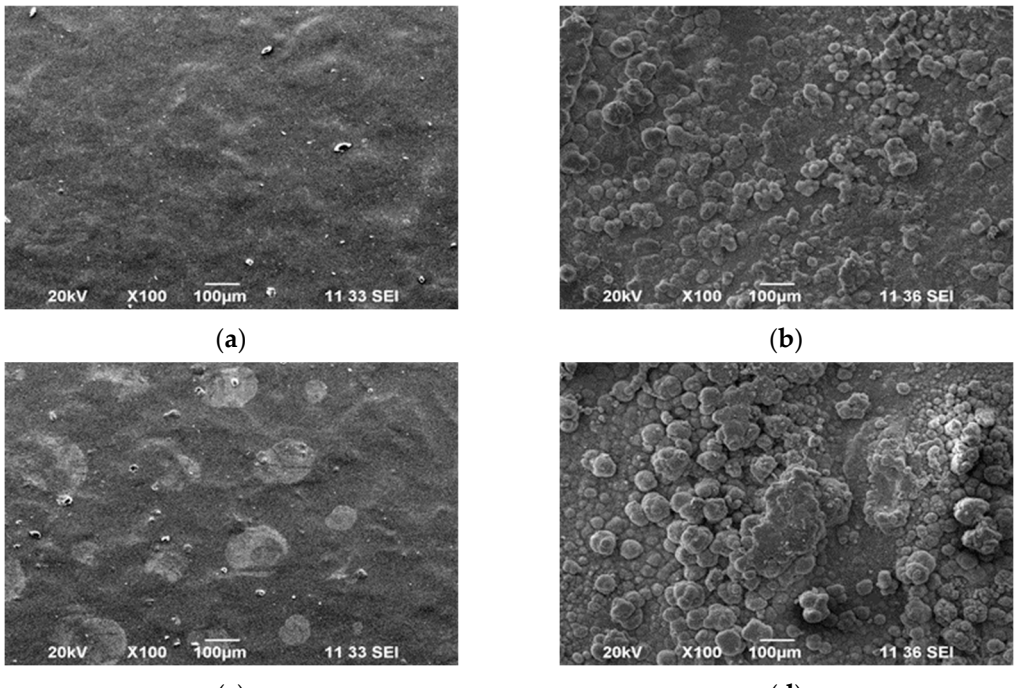

(**a**) (**b**)

(**c**) (**d**)

Figure 3. SEM images of hybrid COS1 (**a**,**b**) and COS2 (**c**,**d**) coatings before (**a**,**c**) and after (**b**,**d**) corrosion treatment in model medium of 5% NaCl solution.

3.3. Cyclic Voltammetry (CVA) Studies

CVA voltammetry studies of ordinary zinc, COS1, and COS2 probes are presented in Figure 4. These tests have been conducted in the starting electrolytes applied for the electrodeposition of ordinary and both hybrid zinc coatings, respectively. It can be registered that the electrodeposition process of the ordinary zinc takes part at much higher cathodic current and begins at more negative potential value compared to both hybrid coatings. This observation confirms that the cathodic deposition of the hybrids is depolarized and occurs at more positive cathodic potentials and much lower cathodic current −0.009 A for COS1 probe and −0.010 A for COS2, respectively. For comparison, the cathodic deposition peak of the zinc is registered at −0.051 A, i.e., its value is about five times higher. These data can be regarded as a sign for the greater deposition rate of the ordinary zinc despite the fact that its cathodic process seems to be overpolarized according to Figure 4.

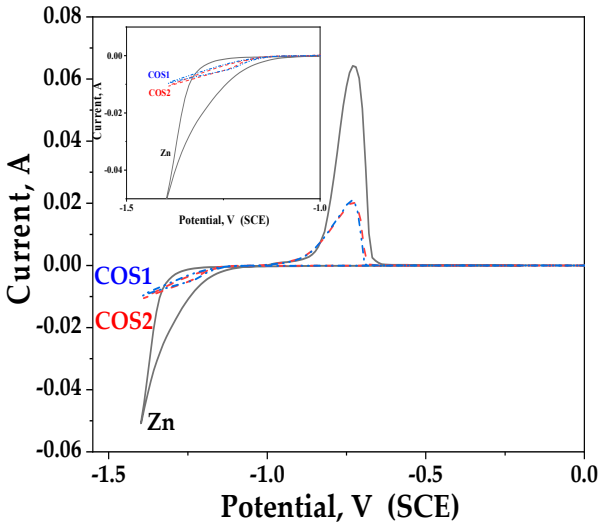

Figure 4. Cyclic voltammetry investigations of both hybrid coatings COS1 and COS2 and of ordinary zinc (Zn).

The anodic regions of all curves present the course of the anodic dissolution process. Their presence confirms also the availability of the electrodeposited coatings on the low-carbon steel substrate. The figure clearly shows that the Zn dissolution peak is the greatest one (0.065 A at −0.725 V) which indicates the presence of greater electrodeposited mass. Contrary to this, the anodic peaks of both hybrids are much lower and practically almost equal −0.021 A. The inset in Figure 4 demonstrates the occurring cathodic processes in more details.

Obviously, the incorporation of COS coated ZnO particles in the starting electrolytes is the reason for this observation. The above mentioned particles are bigger in size compared to the zinc ions and when they electrodeposit on the substrate it is presumed that they will physically block to a certain degree the substrate for the deposition of the free zinc ions. Nevertheless, ZnO particles most probably support the electrodeposition of the zinc ions building hybrid coating with simultaneously incorporated metal, oxide and organic components.

3.4. Potentiodynamic Polarization (PDP) Curves

Potentiodynamic polarization can be defined as accelerated investigation aimed to receive preliminary information about the corrosion behavior of the hybrid coatings (COS1 and COS2, respectively) compared to the ordinary zinc one in the model test medium. The results obtained are shown in Figure 5. Some of the most important electrochemical parameters obtained from the figure are demonstrated in Table 1.

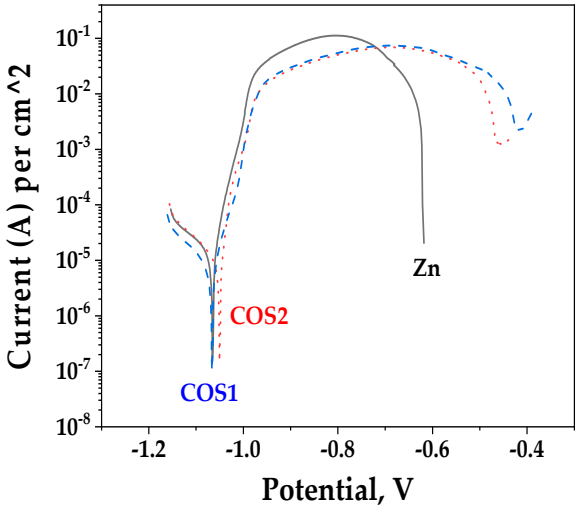

Figure 5. Potentiodynamic polarization curves of both hybrid coatings COS1 and COS2 and of ordinary zinc (Zn).

Table 1. Electrochemical parameters obtained from Figure 5.

Sample	I_{corr}, A·cm^{-2}	E_{corr}, V
Zn	1.7×10^{-5}	−1.07
COS1	8.2×10^{-6}	−1.07
COS2	1.3×10^{-5}	−1.05

As seen from the figure, the corrosion potentials of ordinary zinc and COS1 sample are practically identical. The same parameter of COS2 probe is slightly more positive (see Table 1). The values of the corrosion current densities differ—I_{corr} of ordinary zinc is higher compared to both hybrids. The anodic curve of the usual zinc increases gradually in the zone after the corrosion potential and then shows a maximum at potential of about −0.8 V. Thereafter, the coating complete dissolute in the potential area of about −0.6 V and the bare steel surface appears. Both hybrid zinc-based coatings COS1 and COS2 demonstrate different behavior since their anodic parts are longer compared to that of the ordinary Zn. This result is an evidence that the newly obtained hybrid coatings are more resistive at external anodic polarization. The length of COS1 sample anodic curve is up to about −0.4 V and that of COS2 is until −0.44 V. In the area of the maximal anodic dissolution both hybrid samples characterize with lower maximal current densities in comparison to the same parameter from the zinc curve.

In addition, the anodic curve of COS2 increases rather steeply in the potential area after the corrosion potential (which generally means accelerated dissolution) while for the COS1 sample some deceleration is observed (i.e., the rate in this zone of about −0.1 V partially decreases) and only then increases again.

The observed results can be explained with the hybrid coatings composition as well as the type and quantity of the corrosive products arising during the polarization. The corrosion product that appeared in that test medium is expected to be mainly zinc hydroxide chloride $Zn_5(OH)_8Cl_2 \cdot H_2O$, which is characterized by a very low product of solubility value [24]. Its availability leads to better protection of the low-carbon steel substrate since it impedes partially the penetration of the chloride ions deeply inside. The presence of COS coated ZnO particles in the zinc matrix also improves the protective characteristics of the coating and supports the appearing of "barrier effect" against the chloride ions. In general, it might be concluded that the presence of COS coated ZnO particles influences positively the corrosion characteristics of the ordinary zinc at conditions of external potential, i.e. at accelerated corrosion test. This effect can be stated from the presence of longer anodic curves and lower corrosion current densities compared to the zinc. This observation can

be regarded as a parameter for their better stability and increased corrosion resistance in model medium containing corrosion activators (chloride ions).

3.5. Polarization Resistance (Rp) Measurements

The results from the Polarization resistance measurements received after 45 days' immersion period of the tested samples in 5% NaCl solution are shown in Figure 6. The ordinary zinc coating demonstrates on average Rp values of about 780–850 ohm·cm^2 during this period, and the maximum can be observed after 25 days' investigation.

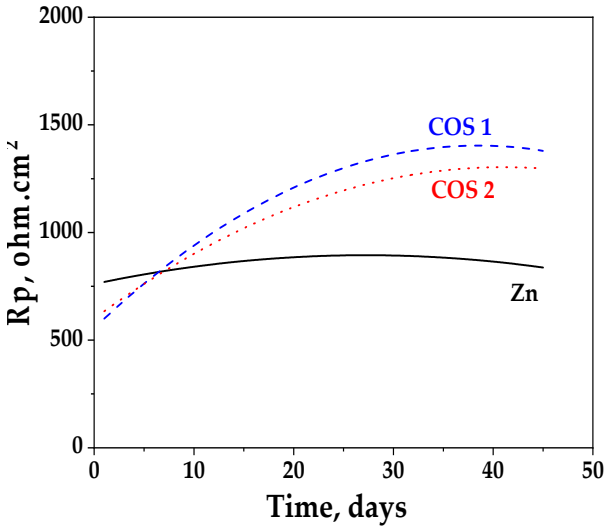

Figure 6. Polarization resistance of ordinary zinc (Zn) and hybrid coatings COS1 and COS2.

The experimental maximal Rp values for COS1 (~1400 ohm·cm^2) and COS2 (~1310 ohm·cm^2) are about twice as high compared to the zinc. This means that the presence of the COS-coated ZnO particles in the metal matrix of the zinc positively influences the anticorrosion behavior in that medium. The influence of the embedded particles is weaker expressed for the COS2 sample. According to the obtained results it is obvious that both samples demonstrate their highest polarization resistance after 35 days' immersion in the model medium.

These results could be interpreting with the existence of a layer of corrosion product/s in that model medium, in comparison with some other studies [24]. Generally, this is the compound zinc hydroxide chloride (ZHC) with a low product of solubility value which ensures additional protection against the corrosion activators, creating a "barrier" layer. The presence of COS-coated ZnO particles seems to improve this effect.

Generally, the local corrosion process of the ordinary zinc coating (dissolution) in chloride-containing medium occurs in selected areas. The latter gradually develop/penetrate deeply inside and, after a certain time, will reach the low-carbon steel substrate. Zinc corrosion products, for example, zinc hydroxide chloride (ZHC)—$Zn_5(OH)_8Cl_2 \cdot H_2O$—also forms, covering some areas of the surface.

In the cases when polymer particles are present in the metal matrix, the corrosion process will localize in the metal zones surrounding the particles. As a result, accelerated dissolution of zinc will begin, and a "mixed" film consisting of ZHC (sometimes also with other zinc-based corrosion products like, for example, zincite, etc.) and the particles will occur. In this case, the corrosion process will take place around the particles and the probability of obtaining local deep penetrations of the coating will be reduced/minimized.

Therefore, such a development of the process will increase the probability that local corrosion will partially transform into a general one, which in turn will reduce the possibility of destruction deeply inside. When general corrosion occurs, surface damages are well visible, which means that the prevention can be realized in time.

However, when the immersion test ("open-circuit" conditions) is applied, the formation of ZHC occurs differently contrary to the case of the external polarization (the latter is accelerated test).

3.6. Surface Topography and Wettability

It is well known that more hydrophobic surface is beneficial for the anti-corrosion protection of metals. For that reason, wettability of the samples was evaluated by measuring the water contact angle (Figure 7). As seen, COS1 coatings were more hydrophobic than COS2, which suggests better expressed corrosion resistance and protective ability.

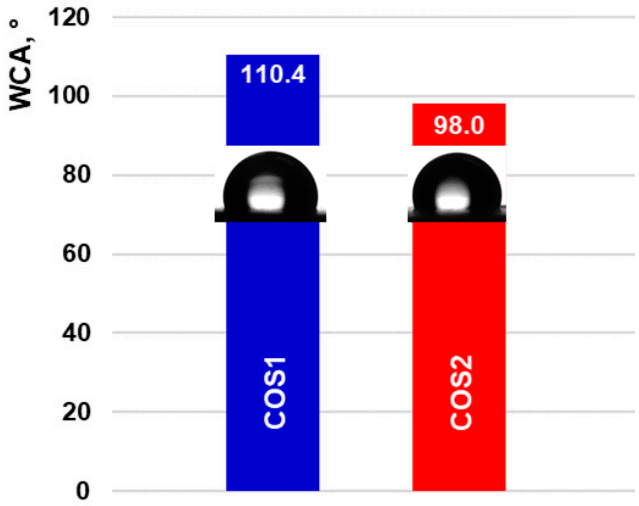

Figure 7. Water contact angle measurements and representative images of the droplets onto hybrid coatings of COS1 (blue) and COS2 (red).

The surface topography images of the non-treated and the corrosion-treated hybrid samples evaluated by AFM are shown in Figure 8. Obviously, the non-treated hybrid samples COS1 and COS2 show smooth and uniform surface of coated material rarely enclosing domains of size 0.2–0.6 μm. Some of the embedded COS-coated ZnO particles are well visible, confirming the availability of a hybrid coating.

Oppositely, the corrosion-treated hybrid samples COS1T and COS2T show very rough and non-uniform surface of coated material mainly containing large domains of size 2–5 μm, which are the newly appeared corrosion products as a result of the treatment.

The roughness values for all samples are summarized in Table 2.

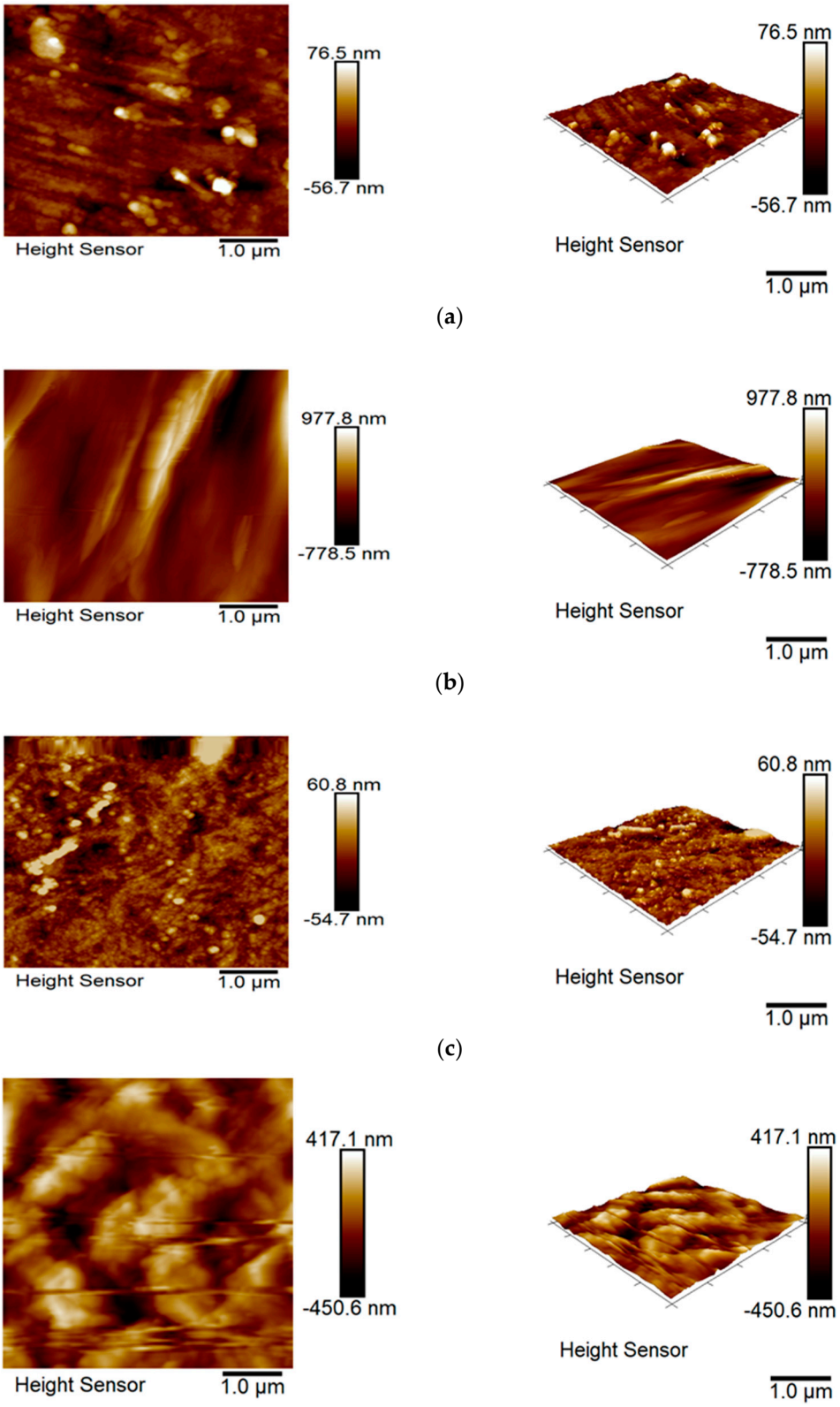

Figure 8. AFM tapping mode 2D and 3D images of the hybrid samples of: (**a**) COS1; (**b**) COS1T; (**c**) COS2, and (**d**) COS2T.

Table 2. Roughness parameters from AFM surface topography images.

Sample	COS1	COS1T *	COS2	COS2T *
Image (μm × μm)	5 × 5	5 × 5	5 × 5	5 × 5
Rq (nm)	15.9	213.0	14.7	128.0
Ra (nm)	10.8	153.0	11.0	104.0

* T—corrosion treatment.

3.7. XRD Studies

The diffractograms of the investigated samples were recorded in a standard omega–2 theta diffractometer geometry. In this way, data are obtained on the distribution of crystalline phases in the coating relative to the normal to the substrate. If, for example, a Zn polycrystalline powder sample is studied (prepared according to all standards of sample preparation), the probability of occurrence of all crystal planes would be equally likely. The type of such diffractograms is presented in Figure 9.

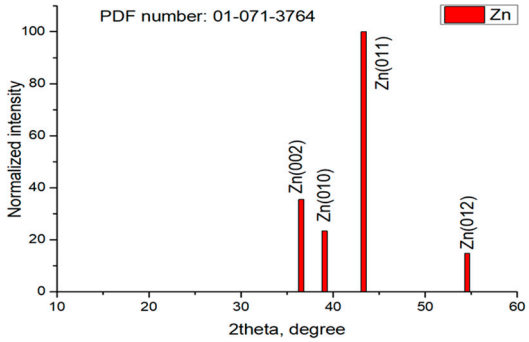

Figure 9. XRD pattern of Zn polycrystalline powder sample.

When obtaining thin-film coatings (for example, during electrodeposition), this is often not the case. The electrodeposition process is influenced by many factors such as potential, current density, temperature, various types of additives, stirring, etc. In the coatings obtained by us, these effects are also present. Under the same conditions but with different amounts of COS-coated ZnO particles concentration in the starting electrolyte, a preferential growth of different crystal planes of the zinc crystals can be observed—Figure 10a,b. The diffractograms show that the intensity of the substrate peak is comparable for both samples, which means that they are approximately of the same thickness. Moreover, at both dopant concentrations, the growth along (002) planes is strongly suppressed, as a result of which its corresponding diffraction peak is almost invisible. Examining the intensity distribution further, it can be seen that at additive concentrations of 0.02 wt.% COS-coated ZnO particles in the starting electrolyte, the growth is stimulated along the crystal plane (010), and at 0.04—along the crystal plane (011). It is important to note that in this diffraction geometry, the growth of the zinc crystals relative to the substrate normal is observed. Thereafter, a rough approximation (guess) can be made of the growth of the zinc crystal relative to its habit (crystal shape). This would help more easily to navigate the way it grows on the surface of the substrate. The shape of the crystals was generated according to their symmetry in a program for visualization of crystal structures and shapes—VESTA [25].

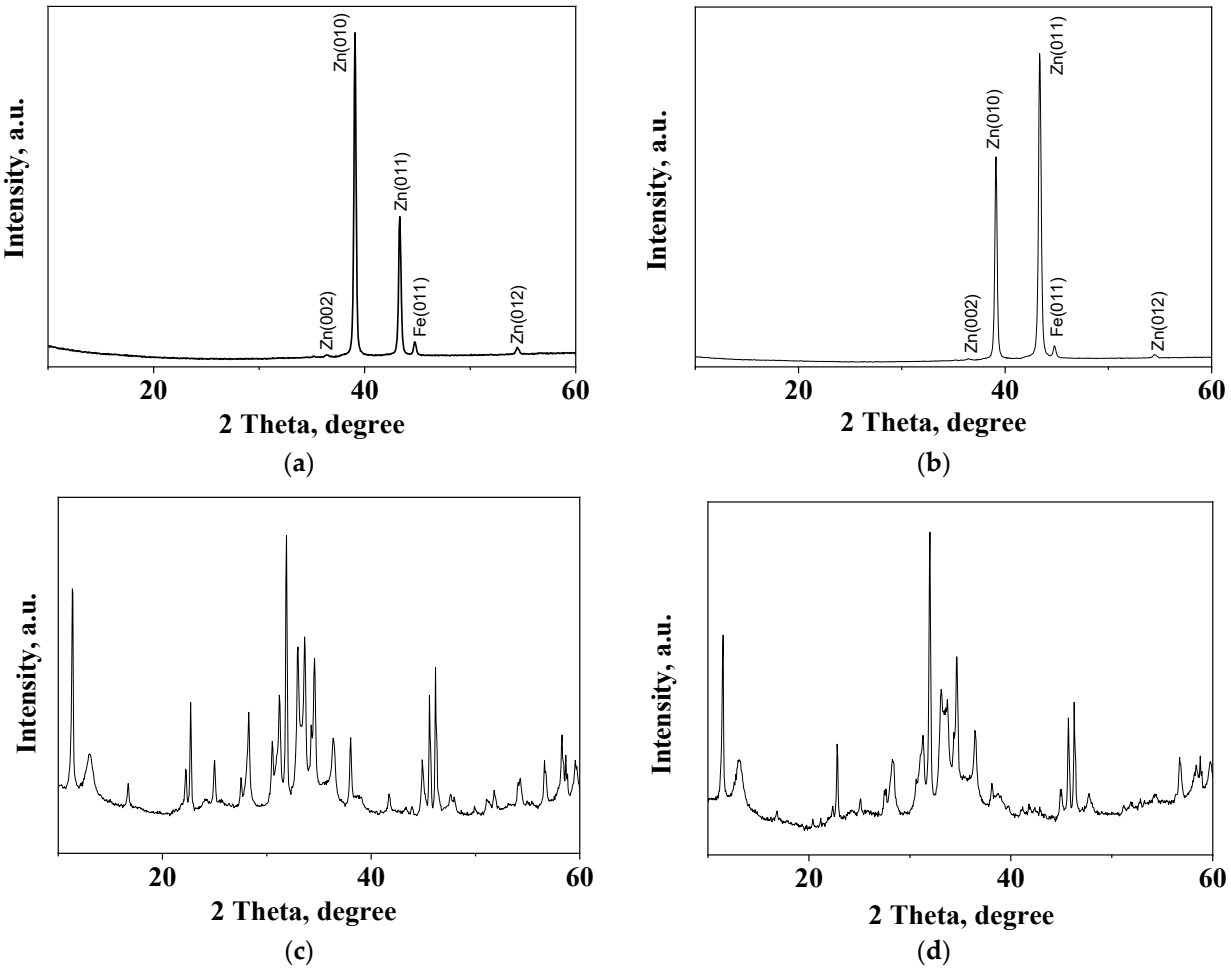

Figure 10. XRD patterns of ordinary zinc (Zn) and hybrid coatings COS1 (**a**), COS2 (**b**), COS1T (**c**), COS2T (**d**).

In Figure 11, the crystalline forms of a zinc crystal are shown and are oriented with respect to the substrate normal which is directed upwards. The conclusions drawn could give us an argument for better understanding of the manifested differences in the anti-corrosion properties of the coating, since it is expected that different planes in the crystal have different properties/susceptibility to corrosion.

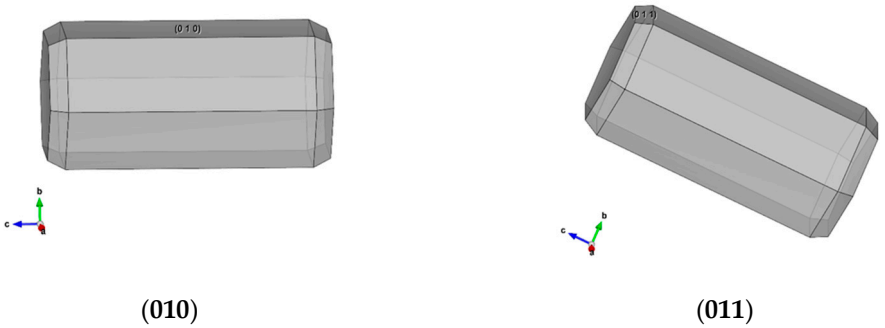

(**010**) (**011**)

Figure 11. Difference in the orientations of the zinc substrates as a consequence of changing the dopant concentrations.

After corrosion treatment, the diffractograms change, demonstrating many additional peaks, the latter being characteristic for the newly appeared corrosion products like zinc hydroxide chloride (ZHC), hydrozincite (HZ)—most probably as a result of ZHC interaction

with air—and zincite (Z). Additional peaks indicating the presence of NaCl also appear in the patterns—Figure 10c,d. Some of the characteristic peaks for Zn, ZHC, HZ, and Z are shown in Table 3.

Table 3. Some characteristic peaks of the corrosion products registered.

Sample	Peaks, 2 Theta Degree
Zn	39.08; 39.11; 43.33; 43.35; 54.46
ZHC	11.36; 16.69; 22.23; 22.69; 24.98; 30.52; 31.22; 32.96; 33.63; 34.57; 36.39; 38.02; 43.92; 45.61; 46.20; 48.00; 51.80; 54.30; 58.28; 58.70; 59.58
HZ	13.00; 28.27; 30.52; 31.22; 32.96; 41.72; 45.61; 51.10; 56.64; 58.70; 59.57
Z	34.57; 36.39; 47.60; 56.64

The discussion concerning the influence of the crystallographic orientation on the corrosion behavior has been investigated also by other scientists by testing different materials [26–30].

For example, the relation of corrosion behavior of aluminum on crystallographic orientation has been investigated in four concentrations of hydrochloric acid aqueous solutions. The corrosion behavior is strongly affected from the crystallographic orientation of the planes parallel to the surface. The orientation dependence was varied with the concentration of the solution. While {101} and {111} plane have corrosion resistance in low concentrations of 1.5 mol/L and 2.9 mol/L HCl, the pitting rate on {111} plane was highest in high concentrations of 5.8 mol/L and 11.6 mol/L HCl [26,27].

The influence of crystallographic orientation on the corrosion was investigated for pure magnesium in 0.1 N HCl. The corrosion depth and orientation of surface features were mapped against crystallographic orientation for many off-principal magnesium crystals. The most corrosion resistant orientation has been confirmed [28].

The corrosion behavior of magnesium single crystals with various crystallographic orientations was also examined. The effects of surface orientation on the corrosion behavior were characterized with potentiodynamic polarization and potentiostatic tests as well as electrochemical impedance spectroscopy measurements in 3.5 wt.% NaCl solution. The results obtained from potentiostatic tests were in agreement with the trend in potentiodynamic polarization tests as a function of rotation angle [29].

A highly corrosion-resistant Mg-Zn-Y-Al alloy featuring an α-Mg/LPSO two-phase multimodal microstructure was investigated. The alloy showed orientation-dependent corrosion behavior; the longitudinal section exhibited a higher corrosion rate than the transverse section. The orientation dependence was attributed to the varying in-plane atomic densities of the crystallographic planes on the longitudinal and transverse sections [30].

3.8. XPS Analysis

The surface compositions and chemical states of COS-coated ZnO hybrid layer electrodeposited on low-carbon steel were investigated by XPS method. The XPS spectra reveal that the surface consists of C, O, Zn as well as Cl and Na (only for the corrosion-treated samples)—(Table 4). The C1s spectra of the corrosive untreated surface was asymmetric and corresponded to three binding energies: 285.0 eV for adventitious carbon, 286.2 eV for C–O bond, and 288.8 eV for carboxyl groups, describing from COS. Another peak at 283.6 eV is also observed in sample COS1, which is due to carbide species (Figure 12a). The O1s signal consists of three peaks, which can be associated with oxygen in zinc oxide lattice at 530.3 eV, carboxyl groups at 531.8 eV, and C-O bond at 533.0 eV (Figure 12b). Figure 12c shows Zn2p spectra of untreated and treated surfaces of samples after immersion in 5% NaCl solution with binding energies of 1021.8 eV and 1022.1 eV, respectively.

Table 4. XPS results of quantitative composition of ZnO/COS layer.

Samples	C, at. %	O, at. %	Zn, at. %	Cl, at. %	Na, at. %
COS1	71.7	20.2	8.1	-	-
COS2	51.3	33.7	15.0	-	-
COS1T	27.0	29.0	15.6	16.5	11.9
COS2T	28.2	36.6	20.6	8.6	6.0

T—corrosion treatment.

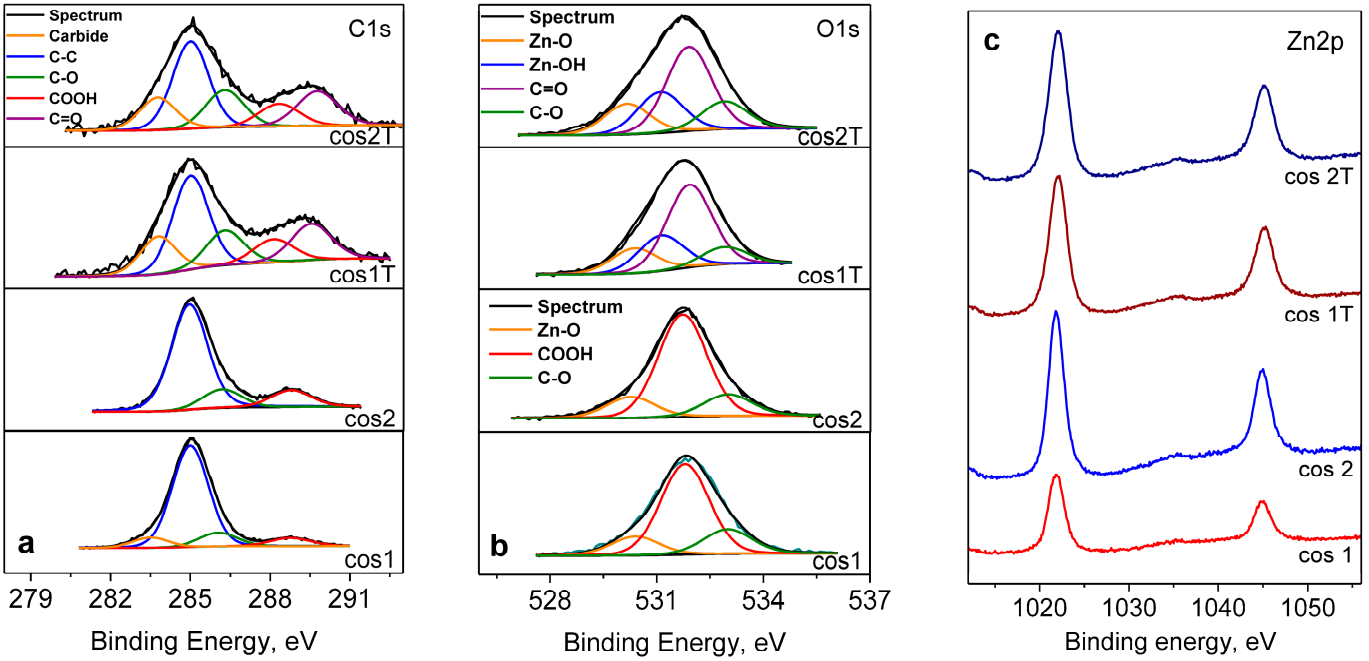

Figure 12. Deconvolution of C1s (**a**) and O1s (**b**) core level spectra and photoelectron spectra of Zn2p (**c**) of ZnO/COS hybrid layer.

For a more precise determination of the state of the zinc, the modified Auger parameter was also calculated, and its values are 2009.3 eV and 2010.6 eV. From the Auger spectra of zinc Zn LMM and the calculation of the Auger parameter, it is established that zinc is in the 2^+ oxidation state, and for treated samples in addition to ZnO, $Zn(OH)_2$ is also observed [31].

XPS analysis shows that the shape of the spectra of the chemical elements consisting on the surface before and after corrosion tests are different, and there are chemical shifts of binding energies. The spectrum of C1s decomposes into one more component, which is attributed to the carbonyl groups. The change in the O1s spectra is the presence of $Zn(OH)_2$ and carbonyls groups as well. On the surface is the registered amount of Cl and Na, because of the corrosion treatment in the model medium. There is no iron observed on the surface, which shows that the layers cover the low-carbon steel substrate well and can be used as anti-corrosion coatings.

4. Conclusions

The successful obtaining of electrodeposited hybrid zinc coatings containing COS-coated ZnO particles in the metal zinc matrix with a potential for low-carbon steel protection in aggressive corrosion environment was reported. The incorporation of these particles in the zinc allows the formation of hybrid coatings with nearly homogeneous ZnO distribution from dispersions stabilized against aggregation.

SEM and AFM characterization revealed the disposal of COS-coated ZnO particles near or directly on the coatings' surface, which made them able to ensure better protection

against the corrosive agents. The contact angle measurements proved that the hybrid coating with low content of COS-coated ZnO particles (COS1) is more hydrophobic compared to the hybrid coating with higher ZnO content.

Hybrid zinc coatings provided enhanced corrosion protection for the low-carbon steel in model medium of 5% NaCl solution during a prolonged period of 45 days compared to the ordinary zinc. Their protective characteristics are better expressed, most probably due to the appearance of a "mixed" layer consisting mainly of zinc hydroxide chloride (ZHC) and COS-coated ZnO particles. This mixed layer ensures a "barrier" effect against the aggressive Cl^- ions presenting in the test solution and impedes their penetration deeply inside the coating. The combined anticorrosion effect of COS and COS-coated ZnO particles on the corrosion process was stronger expressed in the case of the lower ZnO content (COS1 sample), most probably due to the more suitable from a corrosion point of view crystallographic orientation of the electrodeposited hybrid coatings. It seems that the crystallographic orientation (010) provides a denser coverage of the steel substrate, unlike (011) where some cracks and gaps are likely to appear through which the corrosive agents can reach the pad more easily.

Author Contributions: Conceptualization, O.S. and N.B. (Nikolai Boshkov); Data curation, O.S. and N.B. (Nelly Boshkova); Formal analysis, G.G., G.A., M.S., O.S., S.A.-V., N.B. (Nikolai Boshkov) and N.B. (Nelly Boshkova); Funding acquisition, N.B. (Nikolai Boshkov) and O.S.; Investigation, N.B. (Nelly Boshkova), G.G., G.A., M.S., O.S. and S.A.-V.; Methodology, N.B. (Nelly Boshkova), G.G., O.S. and N.B. (Nikolai Boshkov); Writing—review and editing G.G., O.S., N.B. (Nelly Boshkova) and N.B. (Nikolai Boshkov). All authors have read and agreed to the published version of the manuscript.

Funding: This research received no external funding.

Data Availability Statement: The original contributions presented in the study are included in the article, further inquiries can be directed to the corresponding author.

Acknowledgments: Research equipment of the Distributed Research Infrastructure INFRAMAT, part of the Bulgarian National Roadmap for Research Infrastructures, supported by the Bulgarian Ministry of Education and Science was used for some investigations in the present study.

Conflicts of Interest: The authors declare no conflicts of interest.

References

1. Koch, G.; Brongers, M.; Thomson, N.; Virmani, Y.; Payer, J. *Corrosion Cost and Preventive Strategies in the United States*; NACE International: Houston, TX, USA, 2016.
2. Zhang, X.G. *Corrosion and Electrochemistry of Zinc*; Plenum Press: New York, NY, USA, 1996; ISBN 978-1-4757-9877-7.
3. Popoola, P.A.I.; Malatji, N.; Fayomi, O.S. Fabrication and properties of zinc composite coatings for mitigation of corrosion in coastal and marine zone. In *Applied Studies of Coastal and Marine Environments*; InTech: London, UK, 2016; Volume 32, pp. 137–144.
4. De La Fuente, D.; Castano, J.G.; Morcillo, M. Long-term atmospheric corrosion of zinc. *Corros. Sci.* **2007**, *9*, 1420–1436. [CrossRef]
5. Maniam, K.K.; Paul, S. Corrosion performance of electrodeposited zinc and zinc-alloy coatings in marine environment. *Corros. Mater. Degrad.* **2021**, *2*, 163–189. [CrossRef]
6. Sorensen, P.A.; Kiil, S.; Dam-Johansen, K.; Weinell, C.E. Anticorrosive coatings: A Review. *J. Coat. Technol. Res.* **2009**, *6*, 135–176. [CrossRef]
7. Zhang, H.; Chen, B.; Banfield, J.F. Particle size and pH effects on nanoparticle dissolution. *J. Phys. Chem. C* **2010**, *114*, 14876–14884. [CrossRef]
8. Srivastava, M.; Srivastava, S.K.; Ji, N.G.; Prakash, R. Chitosan based new nanocomposites for corrosion protection of mild steel in aggressive chloride media. *Intern. J. Biolog. Macromol.* **2019**, *140*, 177–187. [CrossRef]
9. Azizi, M.; Schneider, W.; Plieth, W. Electrolytic co-deposition of silicate and mica particles with zinc. *J. Solid State Electrochem.* **2005**, *9*, 429–437. [CrossRef]
10. Xia, X.; Zhitomirsky, I.; McDermid, J.R. Electrodeposition of zinc and composite zinc-yttria stabilized zirconia coating. *J. Mater. Process. Technol.* **2009**, *209*, 2632–2640. [CrossRef]
11. Adriana, V.; Simona, V.; Aurel, P.; Caius, B.; Liana, M.M. Electrodeposited Zn–TiO_2 nanocomposite coatings and their corrosion behavior. *J. Appl. Electrochem.* **2010**, *40*, 1519–1527.
12. Behzadnasab, M.; Mirabedini, S.M.; Kabiri, K.; Jamali, S. Corrosion performance of epoxy coatings containing silane treated ZrO_2 nanoparticles on mild steel in 3.5% NaCl solution. *Corr. Sci.* **2011**, *53*, 89–98. [CrossRef]

13. Mohammad, B.; Mahamood, A.; Mehdi, A. Cu-Zn-Al_2O_3 nanocomposites: Study of microstructure, corrosion, and wear properties. *Int. J. Met. Mater.* **2017**, *24*, 462–472.
14. Kamburova, K.; Boshkova, N.; Boshkov, N.; Radeva, T. Composite coatings with polymeric modified ZnO nanoparticles and-nanocontainers with inhibitor for corrosion protection of low carbon steel. *Colloids Surf. A Physicochem. Eng. Asp.* **2021**, *609*, 125741. [CrossRef]
15. Romero, R.; Martin, F.; Ramos-Barrado, J.R.; Leinen, D. Study of different inorganic oxide thin films as barrier coatings against the corrosion of galvanized steel. *Surf. Coat. Technol.* **2010**, *204*, 2060–2063. [CrossRef]
16. Lopez Ibanez, R.; Romero, R.; Martın, F.; Ramos-Barrado, J.R.; Leinen, D. ZnO thin films on aluminized steel by spray pyrolysis. *Surf. Interface Anal.* **2006**, *38*, 789–792. [CrossRef]
17. Tang, F.; Uchikoshi, T.; Sakka, Y. Electrophoretic deposition behavior of aqueous nanosized zinc oxide suspensions. *J. Am. Ceram. Soc.* **2002**, *85*, 2161–2165. [CrossRef]
18. Boshkova, N.; Kamburova, K.; Radeva, T.; Simeonova, S.; Grozev, N.; Shipochka, M.; Boshkov, N. Comparative corrosion characterization of hybrid zinc coatings in Cl^--contaning medium and artificial sea water. *Coatings* **2022**, *12*, 1798. [CrossRef]
19. Anwar, S.; Khan, F.; Zhang, Y.; Caines, S. Zn composite corrosion resistance coatings: What works and what does not work? *J. Loss Prev. Process Ind.* **2021**, *69*, 104376. [CrossRef]
20. Zhang, X.; Liang, J.; Liu, B.; Peng, Z. Preparation of superhydrophobic zinc coating for corrosion protection. *Colloids Surf. A Physicochem. Eng. Asp.* **2014**, *454*, 113–118. [CrossRef]
21. Patel, A.K.; Michaud, P.; de Baynast, H.; Grédiac, M.; Mathias, J.D. Preparation of chitosan-based adhesives and assessment of their mechanical properties. *J. Appl. Polym. Sci.* **2013**, *127*, 3869–3876. [CrossRef]
22. Mati-Baouche, N.; Elchinger, P.H.; de Baynast, H.; Pierre, G.; Delattre, C.; Michaud, P. Chitosan as an adhesive. *Eur. Polym. J.* **2014**, *60*, 198–212. [CrossRef]
23. Varma, A.J.; Deshpande, S.V.; Kennedy, J.F. Metal complexation by chitosan and its derivatives: A review. *Carbohydr. Polym.* **2004**, *55*, 77–93. [CrossRef]
24. Kamburova, K.; Boshkova, N.; Boshkov, N.; Radeva, T.; Atanasova, G. Corrosion protection of electrogalvanised steel by application of non-conducting polyaniline-silica particles. *Trans. IMF* **2021**, *99*, 181–187. [CrossRef]
25. Momma, K.; Izumi, F. Vesta 3 for three-dimensional visualization of crystal, volumetric and morphology data. *J. Appl. Crystallogr.* **2011**, *44*, 1272–1276. [CrossRef]
26. Takayama, Y.; Sato, M.; Watanabe, H. *Crystallographic Orientation Dependence of Corrosion Behavior of 5N Purity Aluminum in Different Concentrations of HCl Aqueous Solutions*; Weiland, H., Rollett, A.D., Cassada, W.A., Eds.; ICAA13 Pittsburgh; Springer: Berlin/Heidelberg, Germany, 2012; pp. 391–396.
27. Takayama, Y.; Nohara, K.; Kato, H. Influence of Crystallographic Orientation on Corrosion Behavior of 5N Purity Aluminum. In Proceedings of the 12th International Conference on Aluminium Alloys, Yokohama, Japan, 5–9 September 2010; pp. 1469–1474.
28. Liu, M.; Qiu, D.; Zhao, M.-C.; Song, G.-L.; Atrens, A. The effect of crystallographic orientation on the active corrosion of pure magnesium. *Scr. Mater.* **2008**, *58*, 421–424. [CrossRef]
29. Shin, K.S.; Bian, M.Z.; Nam, N.D. Effects of Crystallographic Orientation on Corrosion Behavior of Magnesium Single Crystals. *JOM* **2012**, *64*, 664–670. [CrossRef]
30. Yamasaki, M.; Shi, Z.; Atrens, A.; Furukawa, A.; Kawamura, Y. Influence of crystallographic orientation and Al alloying on the corrosion behavior of extruded α-Mg/LPSO two-phase MgZn-Y alloys with multimodal microstructure. *Corros. Sci.* **2022**, *200*, 110237. [CrossRef]
31. Al-Gaashani, R.; Radiman, S.; Daud, A.R.; Tabet, N.; Al-Douri, Y. XPS and optical studies of different morphologies of ZnO nanostructures prepared by microwave methods. *Ceram. Int.* **2013**, *39*, 2283–2292. [CrossRef]